Application of Computational Fluid Dynamics to Compressor Efficiency Improvement

J. R. Lenz
Tecumseh Products Company

E. A. Cooksey
Tecumseh Products Company

Application of Computational Fluid Dynamics to Compressor Efficiency Improvement

James R. Lenz, Edward A. Cooksey
Tecumseh Products Company
Tecumseh, MI

ABSTRACT

The discharge process of a rotary air conditioning compressor was improved through the application of a 3-D computational fluid dynamics analysis. Both re-expansion mass and flow losses were reduced.

INTRODUCTION

Today, more than ever, there is the need for more efficient refrigeration and air conditioning. Compressor manufacturers are working harder and harder to get small gains in energy efficiency ratio (EER). If geometry changes can be made that improve gas handling, it can prove to be an inexpensive way to get efficiency improvements. This paper concentrates on improving the discharge process of a rolling piston type air conditioning compressor.

Figure 1 shows a typical roller and cylinder block. The vane has been removed to help visualize the chamfer on the discharge side of the vane slot. Note also the "notch" in the cylinder block that forms part of the discharge flow path.

There are two ways the discharge process can be improved to increase efficiency. The first way is through reducing flow losses across the discharge port and valve. One way to do this is through increasing the discharge port cross section area. However if the restriction is not in the port but rather under the valve, increasing the valve stop height might be the answer. Furthermore, a larger discharge port diameter adds to the re-expansion volume.

This leads us into the second way the discharge process can be improved, minimization of the re-expansion mass. The re-expansion mass is the quantity of refrigerant left in the cylinder after the discharge process is over. In a rolling piston compressor, it is irreversibly expanded down to suction conditions before the compression process begins. In a reciprocating compressor the re-expansion mass can be approximated by the product of clearance volume (cylinder volume at piston top dead center) times the density of the discharge gas. In a rotary compressor, the re-expansion mass can be defined in a similar way . The volume is mostly discharge port volume. Other contributions come from the wedge of gas formed by the roller, cylinder wall, and vane at the "end-of-discharge" point in the cycle. This is the point in the cycle, when the roller/cylinder contact point meets the discharge port. The chamfer on the discharge side of the vane slot also adds to the re-expansion volume. Remember however that it is the mass in the re-expansion volume that we are concerned with. Any attempt at increasing EER through reduction in re-expansion volume will fail if the refrigerant has more trouble getting out, resulting in more re-expansion mass.

Computational fluid dynamics (CFD) can help resolve some of these issues. In this study, several discharge port design alternatives were evaluated and pressure drop across the port and valve was used to quantify flow losses.

ANALYSIS

The CFD program used here was AVL/FIRE. All analyses in this report used a steady state assumption with stationary boundaries. Though AVL/FIRE has some limited capability for modeling moving boundaries, the motion of the rolling piston compressor geometry was not practical to model. Nonetheless, design improvements that reduce flow losses using state steady assumptions with stationary boundaries would also be expected to reduce flow losses in the unsteady case and hopefully in the real world.

It was decided to concentrate on two points in the discharge process. One is the point were the maximum flow rate is expected through the discharge port. The other point is the end-of-discharge point when the roller/cylinder contact point hits the discharge port. This defines the end the discharge process. Geometry at this point could restrict the last remnant of gas from getting out, resulting in excessive re-expansion mass.

Model Descriptions

Two 3-D volume grids were built, one for each of the above two points in the cycle. These models, shown in Figures 2 and 3 include the gas in the discharge side of the cylinder, in the discharge port, and under the open valve. Finite element models were prepared using PATRAN and translated into an AVL/FIRE data set using a custom Fortran program. The requirements of an AVL/FIRE finite volume grid model are slightly different than for finite element models. Therefore special care must be taken in constructing the finite element model to ensure that it will translate into a usable finite volume grid. All cells must be hexahedrons. Also, the models used in this analysis were "structured grids". All internal cells in a structured grid have exactly six neighbors, and all grid lines that begin at a boundary, continue across to an another boundary without branching. Conceptually, a structured grid is a distorted version of a finite difference grid. Though AVL/FIRE itself will accommodate unstructured grids, the translator program only handles structured grids.

The discharge valve position was determined by a rotary compressor simulation that includes a structural finite element model of the valve and simple thermodynamic relationships that model the pressure in the cylinder and flow through the valve.

The maximum flow point was found by the simulation to be at a crank angle of 135 degrees before top dead center. This defined the geometry for the "max flow" analysis which is shown in Figure 2. The end of the discharge process was found to be at a crank angle of 22 degrees before top dead center. This corresponds to the point in the cycle when the roller contact point meets the edge of the discharge valve port. This is the "end-of-discharge" analysis and is shown in Figure 3.

Boundary Conditions

A velocity condition was specified for the surface defined by the roller. This type of inlet boundary condition fixes the velocity vector at each grid point and the pressures are left as unknowns. The velocity vector was found from the product of the angular velocity and eccentricity of the crankshaft. This assumes the roller is fixed to the eccentric bearing and not rolling at this point in the cycle. This may or may not be true in reality, however a more sophisticated boundary condition would have been much more difficult to model. It is assumed that the final results are not affected much by this simplification. This boundary condition does give the correct volume flow rate.

The outlet boundary was specified as a Von Neumann condition. This specifies that the flow behavior immediately downstream of the outlet surface is the same as in the layer of cells on the upstream side of the outlet. A static pressure is specified at one point on the outlet boundary. The outlet boundary was applied on all external model surfaces downstream of the discharge valve that were not fixed as wall conditions.

Note that on the "max flow" model (figure 2) more of the fluid volume has been added downstream of the discharge valve. This was done because the outlet boundary condition is only an estimate of the flow behavior on that surface. The effect of this uncertainty is reduced if the outlet boundary condition is further downstream. An accurate solution of the flow field in the discharge valve recess is important in determining what effect, if any, the design of this recess has on the flow.

Results

The results of the "end-of-discharge" analysis are shown in Figures 4 and 5. A contour plot of velocity magnitude, Figure 4, shows very little flow in the notch cut into the cylinder bore. The original intent of this notch was to aid the discharge flow process by increasing the effective flow area where the circular port in the main bearing meets the cylinder block. This analysis show that this notch has very little effect on defining the flow in the discharge port. Elimination of this notch would reduce the re-expansion volume with no detrimental effect on efficiency.

Figure 5 shows a contour plot of pressure. These results indicate a 16 psi (110 kPa) pressure difference across the height of the cylinder. This shows that the gas is having trouble getting out at this point in the cycle. Because the chamfer on the discharge side of the vane slot acts as a flow passage at this point, it was decided to try a larger chamfer. Increasing the chamfer from 0.005 inches (0.12 mm) to 0.030 inches (0.76 mm) reduced the predicted pressure difference across the height of the cylinder to 12 psi (83 kPa). This in turn reduces the average density of the gas in the cylinder at this point. It is expected that an even larger chamfer would give further improvement. However a larger chamfer also increases the re-expansion volume. It was unclear whether the reduced gas density, would offset the increased volume, to produce a net decreases in re-expansion mass. It is also difficult to quantify the effect of reduced re-expansion mass on EER. The optimum vane slot chamfer was determined experimentally.

Velocity vectors from the "max flow" analysis are shown in Figure 6. The pressure drop was 11.3 psi (78 kPa). Note the small re-circulation zone in the valve recess. This is a possible source of flow losses. Note also that some sections of the port have low velocity.

In an effort to reduce re-expansion volume, the model was modified to fill in these low velocity regions in the discharge port. The result was a port that is circular at the valve and tapers to a half-circle where it meets the cylinder. The resulting velocity vector plot is shown in figure 7. The pressure drop was reduced to 9.9 psi (68 kPa).

Another modification was tried in which the discharge port was made shorter by increasing the depth of the discharge valve recess. The results of this analysis are shown in figure 8. The pressure drop was 10.3 psi (71 kPa).

In another modification the discharge valve recess was modified by tapering the wall of the recess to 45 degrees. The results are shown in figure 9. Note that the re-circulation is gone. The resulting pressure drop of 11.3 psi (78 kPa) was unchanged from the analysis of the original model.

EXPERIMENTAL RESULTS

The effect of the shorter valve port on EER was evaluated by first running a standard 12,000 BTU/hr (3517 W) rotary compressor to establish a base line at ASRE/T conditions (R22, 45F evaporator, 130F condenser, 95F return gas temperature). The compressor was then modified by machining the port recess to the thinner value. This reduced the port volume by a 40%. Test results showed a 2.3% increase in EER, primarily due to a decrease in power input to the compressor. Testing with production parts confirm these results.

The cylinder wall discharge notch accounts for volume of about 0.0012 cubic inches (0.02 cubic centimeters). A 10,000 BTU/hr (2931 W) rotary was tested at ASRE/T conditions without the notch. It was then re-tested with the notch added. Finally, it was re-tested with the notch filled in. Test results showed an EER increase of approximately 2% without the notch, primarily due to a reduction in power input.

The discharge side vane slot chamfer was evaluated using both a 12,000 BTU/hr (3517 W) and an 8,000 BTU/hr (2345 W) compressor at ASRE/T conditions. The vane slot edge chamfer was incrementally increased, testing after each increase. The experimental results are shown in Figure 10. The best chamfer results gave an EER increase of 2.8%, through a combination of lower watts and increased capacity. It should be noted that is was possible to degrade the performance by excessively increasing the size of the chamfer.

CONCLUSIONS

The computational fluid dynamics analysis is a useful tool in evaluating the effect of discharge flow geometry on compressor efficiency. By studying the velocity vector plots it is possible to determine areas where there is little flow. Improvements in re-expansion volume may be possible by filling in these areas. Various geometry changes can be tried quickly to determine their effect on flow losses.

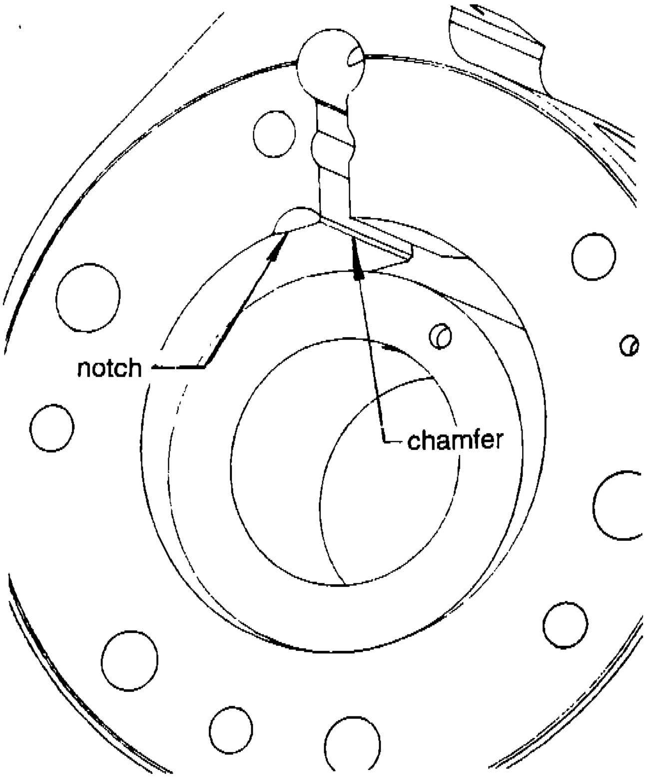

Figure 1 : Roller and Cylinder Block

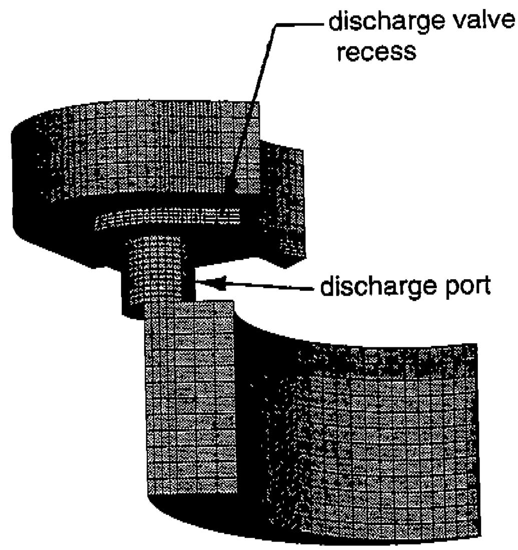

Figure 2 : Max Flow Model

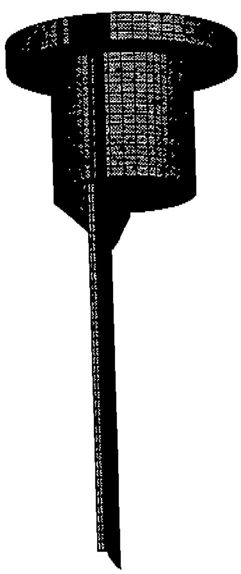

Figure 3 : End of Dischrage Flow Model

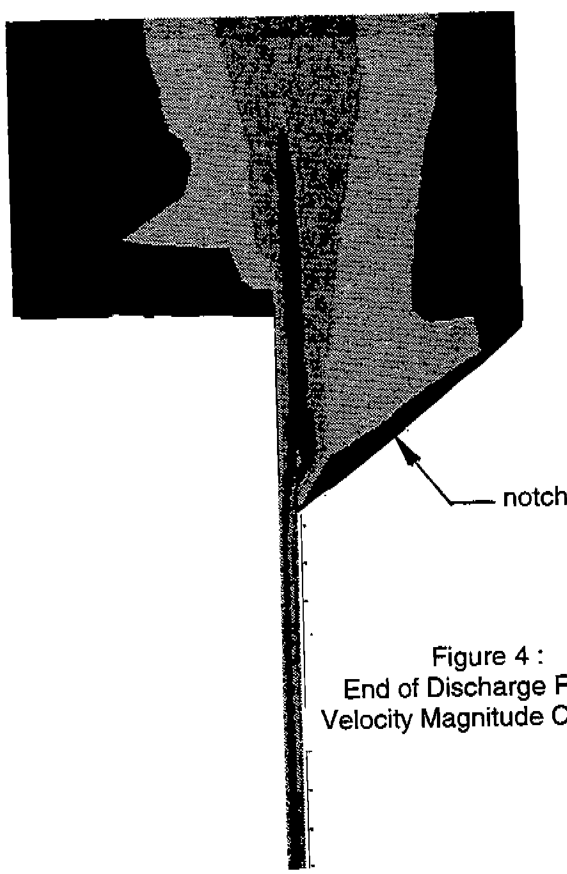

Figure 4 :
End of Discharge Results
Velocity Magnitude Contours

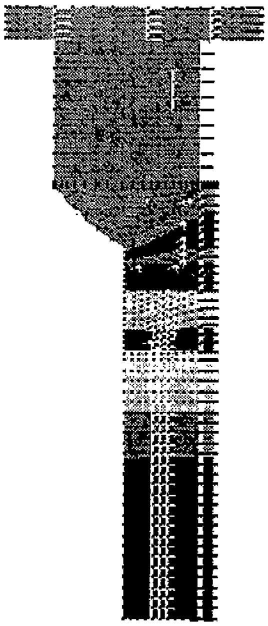

Figure 5 : End of Discharge Results
Pressure Contours

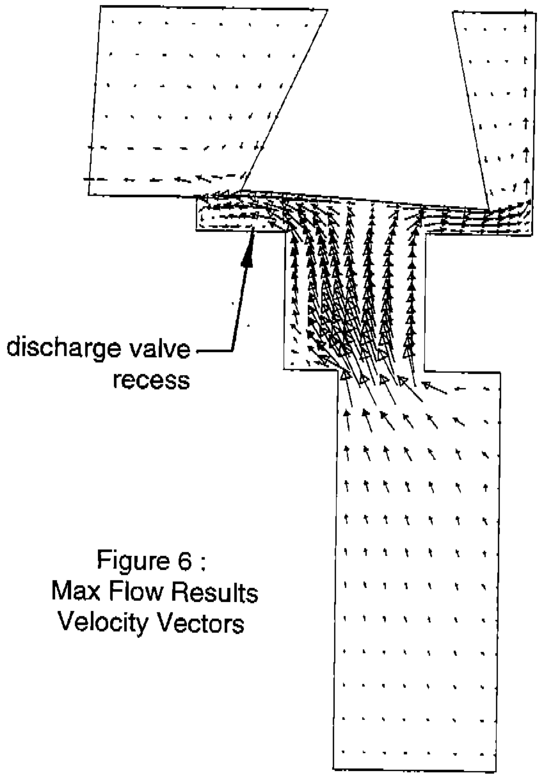

Figure 6 :
Max Flow Results
Velocity Vectors

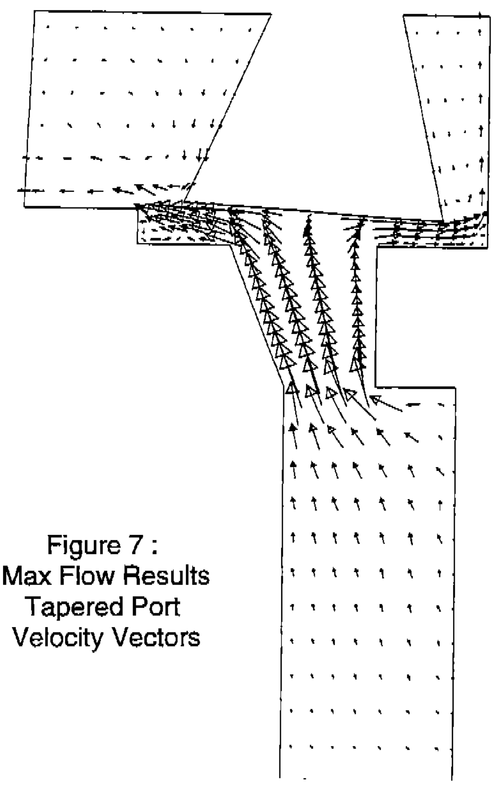

Figure 7 :
Max Flow Results
Tapered Port
Velocity Vectors

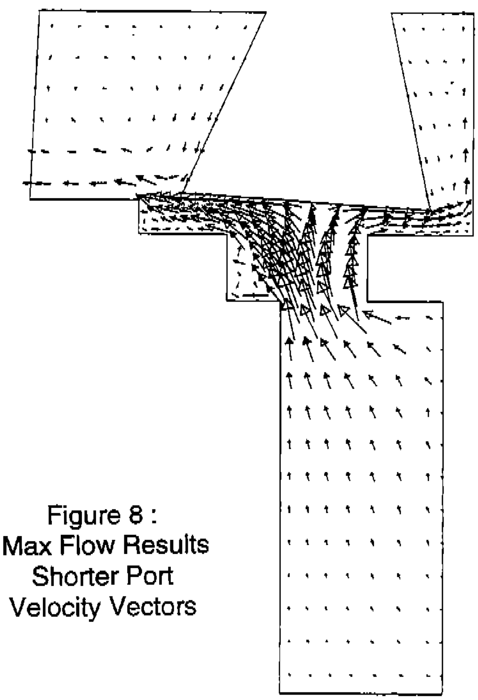

Figure 8 :
Max Flow Results
Shorter Port
Velocity Vectors

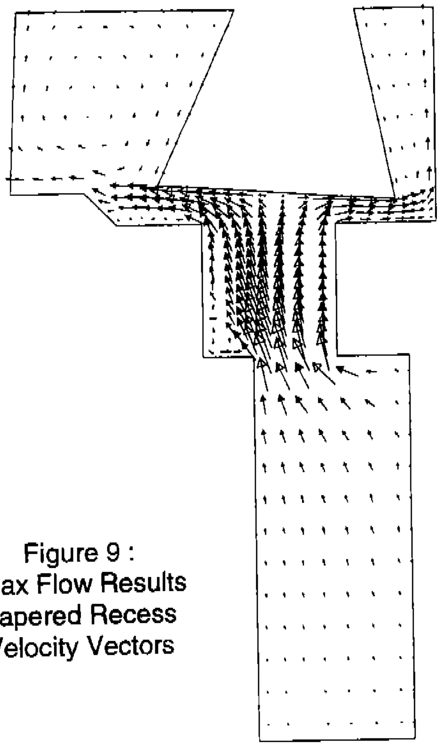

Figure 9 :
Max Flow Results
Tapered Recess
Velocity Vectors

Figure 10 : Test Results with Various Chamfers